Electromagnetic modeling of porphyry systems:
Putting geology back into geophysics from the rock-scale to deposit-scale

Abraham M. Emond[1,4], Erich U. Petersen[2], and Michael S. Zhdanov[3,4], University of Utah, Department of Geology and Geophysics, 135 South 1460 East Room 719, Salt Lake City, UT 84112

[1]aemond@mines.utah.edu, abrahamemond@yahoo.com [2]petersen@earth.utah.edu [3]mzhdanov@mines.utah.edu [4]Center for Electromagnetic Modeling and Inversion, http://www.mines.utah.edu/~wmcemi/

Abstract

Forward geophysical modeling of copper porphyry systems is accomplished using geologic inputs from rock-scale to deposit-scale. This research represents an expansion of the rock properties used for electromagnetic modeling of bulk apparent resistivity. Generalized Effective Medium Theory of Induced Polarization (GEMTIP, Zhdanov, 2006) is used to predict electromagnetic behavior of individual rock types within a porphyry system. For a disseminated sulfide bearing rock GEMTIP theory inputs include sulfide grain size, grain eccentricity, sulfide volume fraction, matrix resistivity, sulfide conductivity, and two empirical parameters: the geometric factor and the relaxation coefficient that must be derived from experimental data. Previous models such as the Cole-Cole model (Cole K.S., 1941) do not incorporate the above rock-scale geologic information.

For deposit scale modeling an Integral Equation Electromagnetic (IEE) forward modeling code developed by the Center for Electromagnetic Modeling and Inversion (CEMI) is used (Zhdanov and Lee, 2005). A new interface to allow modeling of geometrically complex geologic systems was developed for the IEE forward modeling code. This interface allows the 3D modeling of a simplified porphyry model. Both the rock type and associated electric properties (approximate) are used for synthetic data creation. After construction of the general model parameters such as ore body geometry, ore body depth, sulfide volume fraction, and rock resistivity, values can be easily changed to better understand the geophysical response of each parameter. With advances in forward modeling and inversion, detection and discrimination capability will improve for porphyry systems and other geologic targets, leading to greater efficiency in mineral exploration.

Effective resistivity model

The Generalized Effective Medium Theory of Induced Polarization (GEMTIP) allows the rock conductivity to be predicted as function of frequency based on its composition at the grain-scale. The effective resistivity of the polarized inhomogeneous medium composed of a matrix with l types of spherical grains is given by equation (1):

$$\rho_{ef} = \rho_0 \left\{ 1 + \sum_{l=1}^{N} \left\{ f_l m_l \left\{ 1 - \frac{1}{1 + \{ i\omega\tau_l \}^{C_l}} \right\} \right\} \right\}^{-1}, \quad (1)$$

where:

$$m_l = 3\frac{\rho_0 - \rho_l}{2\rho_l + \rho_0} \text{ and } \tau_l = \left\{ \frac{a_l}{2\alpha_0} \{2\rho_l + \rho_0\} \right\}^{1/C_l}.$$

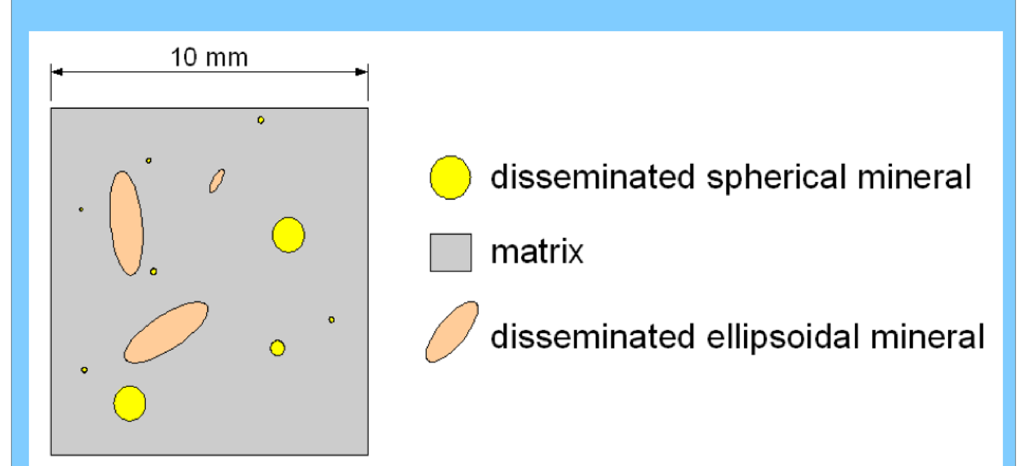

Figure 1: Conceptual illustration of disseminated mineralization. The figure illustrates the basic geometrical input parameters for modeling with the Generalized Effective Medium Theory of Induced Polarization (GEMTIP) including grain size, grain eccentricity (if using an ellipsoidal model) and matrix. The number of minerals is not limited by the GEMTIP theory. Geoelectircal input parameters are described in Table 1.

Table 1: GEMTIP parameter descriptive guide.

variable	units	name	description
ρ_{ef}	Ohm-m	effective resistivity	resulting effective resistivity
ρ_0	Ohm-m	matrix resistivity	matrix resistivity of rock being modeled
f_l	-	grain volume fraction	volume fraction of each grain type
m_l	-	grain chargeability	grain chargeability of each grain type
ω	Hertz	angular frequency	angular frequency of EM signal
τ_l	second	time constant	time constant for each grain
C_l	-	decay coefficient	decay coefficient determined from empirical data
ρ_l	Ohm-m	grain resistivity	resistivity of each grain type
a_l	meter	grain radius	radius of each grain type
α_0	$\frac{\mathrm{Ohm \cdot m^2}}{\mathrm{sec}^{c_l}}$	surface polarizability coefficient	behavior of charges on grain surface determined from empirical data

Porphyry system overview and model development

Figure 2: Areal photo of Lakeshore porphyry copper deposit Pinal County, AZ. The deposit is buried below 150 meters of Tertiary volcanics and sediments and a thin layer of Quaternary gravels. The pit diameter is 0.94 km while the crop circles in the background are 0.75 km in diameter. The elevation of the pit rim is 427 meters above sea level.

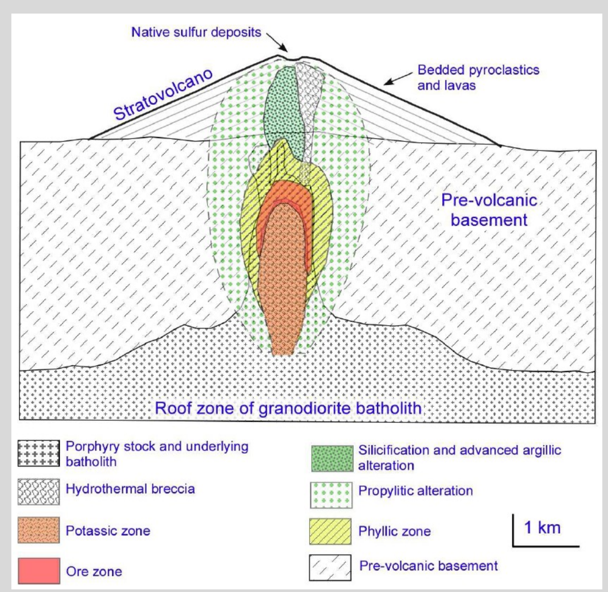

Figure 3: A cross-sectional view of an idealized porphyry copper system shown in magmatic hydrothermal phase (after Sillitoe 1973).

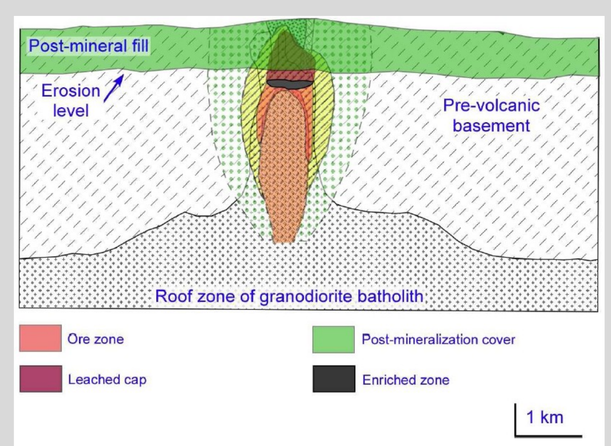

Figure 4: Cross-sectional view of a porphyry copper deposit following weathering and supergene enrichment. Enriched zone shown in dark gray leached cap shown in dark red.

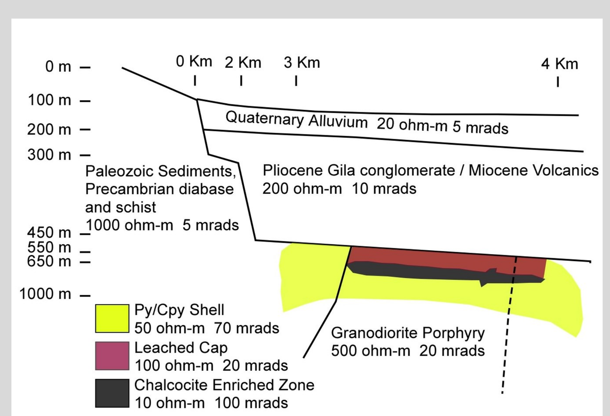

Figure 5: Schematic Southwest US copper porphyry geological/geophysical model (J. Inman, pers. Commun.) containing basic scale information, geologic units, and geoelectrical properties. A normal fault shown on the left side.

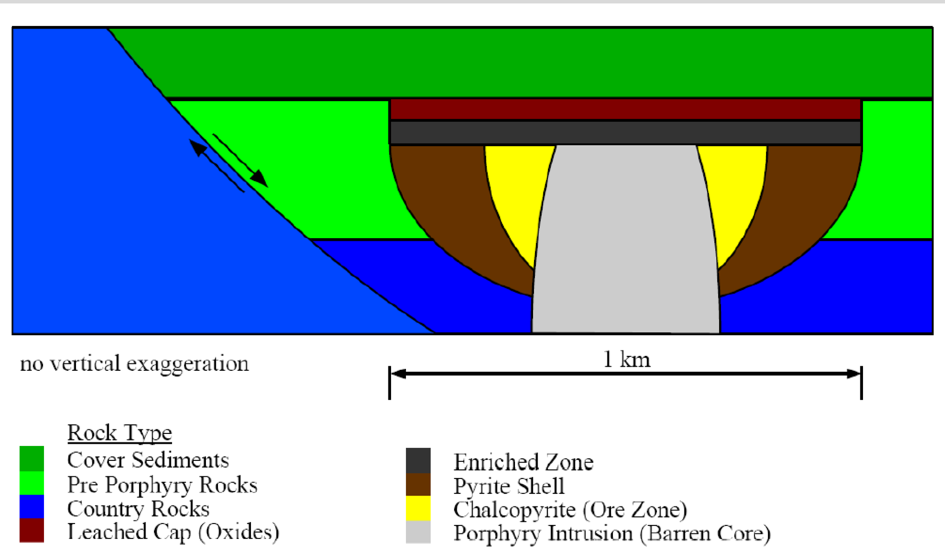

Figure 6: Representation of a simplified porphyry system that can be easily modeled using CEMI IEE codes. This representation incorporates the classic zones of a porphyry deposit and a normal fault.

Rock-scale modeling

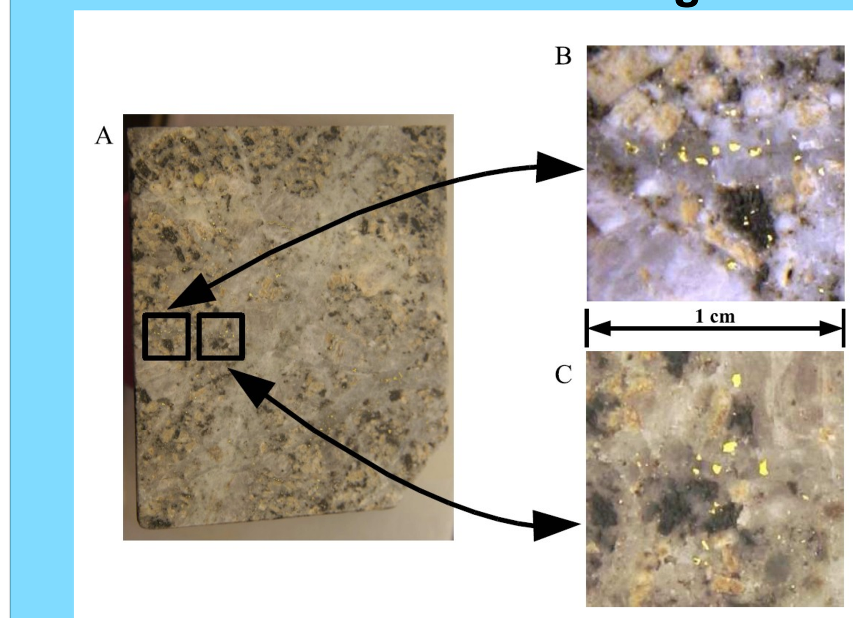

Figure 7: Bingham chalcopyrite ore. A) Hand sample with approximately five percent chalcopyrite (yellow mineral). B,C) Enlargements of insets in A showing disseminated chalcopyrite.

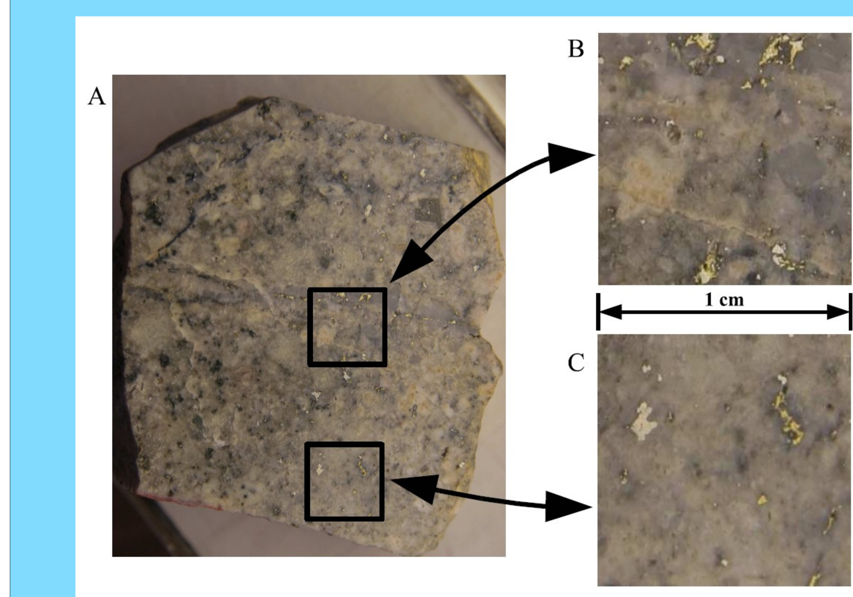

Figure 8: Silver Bell ore. This sample contains approximately 7.5 percent chalcopyrite (yellow gold colored mineral) and 7.5 percent pyrite (pale gold colored mineral). A) Hand sample. B,C) Enlargements of insets in A showing disseminated chalcopyrite and pyrite. This rock would be located between the chalcopyrite and pyrite zones in the Simplified Porphyry Model (Figure 6).

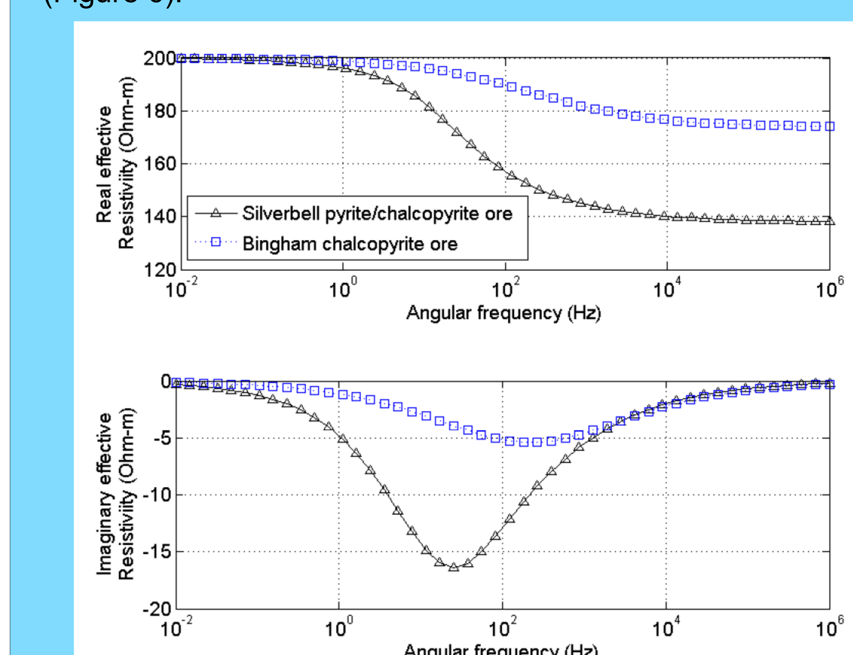

Figure 9: Effective resistivity of Bingham and Silver Bell ores calculated with GEMTIP. A) Real part of total effective resistivity plotted as a function of frequency B) Imaginary part of effective resistivity. The peak IP response occurs when the ratio of the imaginary part of effective resistivity to the real part is largest. As modeled, the peak IP response of the Bingham ore occurs at 500 Hz while the peak IP response of the pyrite containing Silver Bell or occurs at 50 Hz. The difference in in peak IP response frequency could be used for mineral discrimination.

Table 2: GEMTIP parameters for modeling of Bingham and Silver Bell ore.

variable	Bingham	Silver Bell
ρ_{QMP} (Ohm-m)	200	200
$f_{chalcopyrite}$ (%)	5	7.5
f_{pyrite} (%)	-	7.5
ω (Hz)	10^{-2} to 10^{6}	10^{-2} to 10^{6}
$C_{chalcopyrite}$	0.5	0.5
C_{pyrite}	-	0.5
$\rho_{chalcopyrite}$ (Ohm-m)	0.004^a	0.004
ρ_{pyrite} (Ohm-m)	-	0.3^a
$a_{chalcopyrite}$ (mm)	0.5	0.5
a_{pyrite} (mm)	-	0.5
α_0 ($\frac{\mathrm{Ohm \cdot m^2}}{\mathrm{sec}^{c_l}}$)	0.85	0.68

^{a} Nabighian, 1988

Deposit-scale model

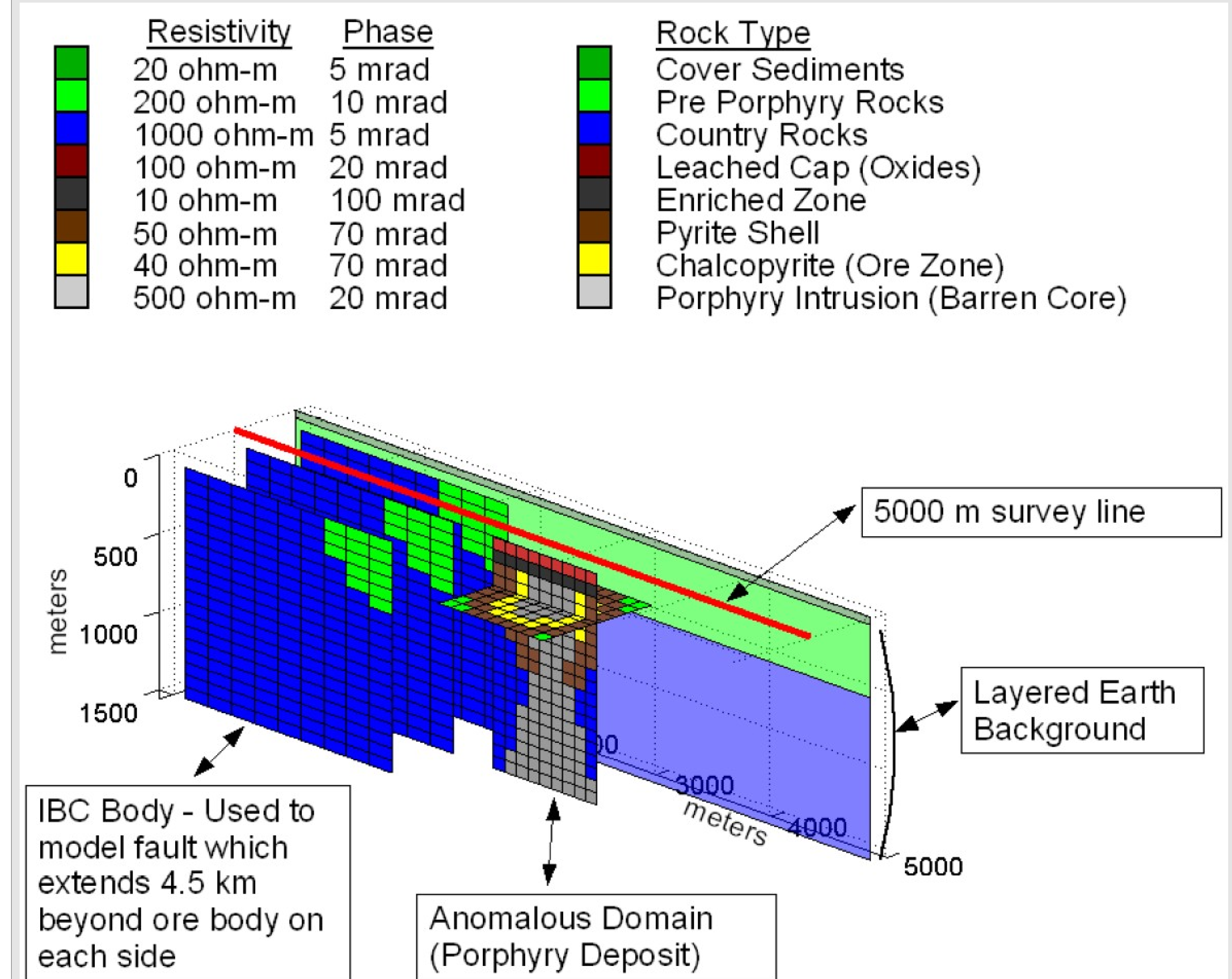

Figure 11: The framework for porphyry forward modeling using the CEMI developed code IBCEM3DIP for MATLAB . The diagram shows the anomalous domain, the location of the survey line, the layered earth background, and the inhomogeneous background (IBC) body for the data presented in figures 12 and 13. For the data presented the enriched zone is 80 meters thick and 150 meters deep. Additionally the geoelectric parameters used for the forward modeling are indicated in the legend. The values used for resistivity and phase are based on the values of the Southwest US copper porphyry geological/geophysical model (Figure 5).

Fit to Empirical Data

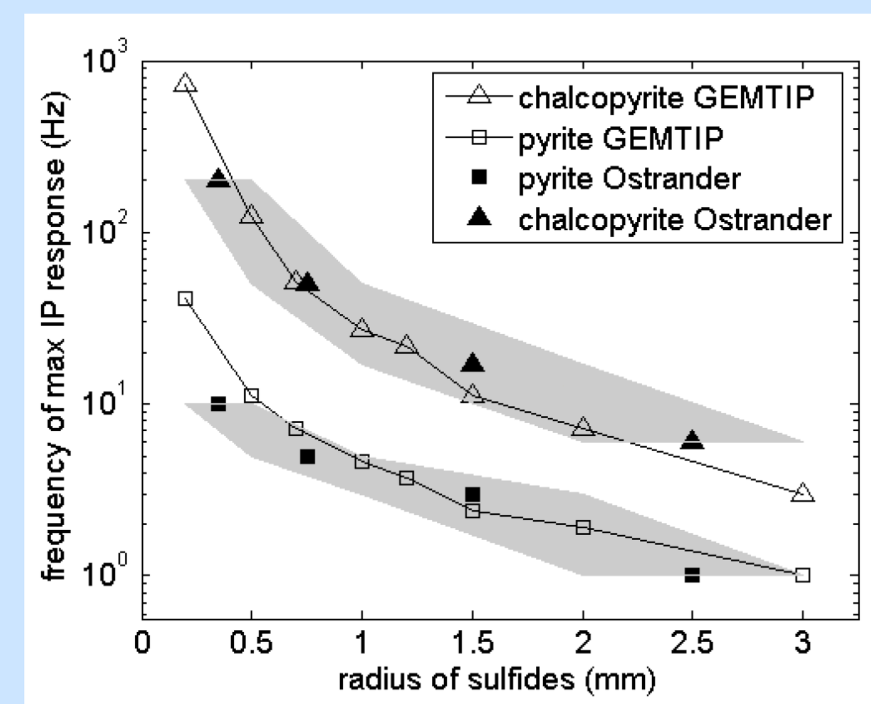

Figure 10: Fit of GEMTIP predicated data with empirical data of Ostrander and Zonge's 1978 rock-scale Induced Polarization study. The good fit of the GEMTIP modeled data with the empirical data indicates GEMTIP can accurately model peak IP response of the rocks measured by Ostrander and Zonge. Ostrander and Zonge studied chalcopyrite and pyrite bearing synthetic rocks with known matrix resistivities. Synthetic rocks bearing either pyrite or chalcopyrite at specific grain sizes were constructed using a cement (matrix) of known resistivity. After the construction of each rock, the frequency of the peak IP response was measured. Results from this study are plotted as the solid squares and solid triangles. The gray shading indicates the range of grain sizes for each measurement of maximum IP response, for example the pyrite synthetic rock plotted at 2.5 mm contains pyrite grains from 2 mm to 3 mm.

Table 3: GEMTIP parameters for fit with Ostrander and Zonge's 1978 data.

variable	CEMI	Ostrander and Zonge
ρ_{ef} (Ohm-m)	-	300 +- 75
ρ_{matrix} (Ohm-m)	300 Ohm-m	-
$f_{chalcopyrite}$	5	-
f_{pyrite}	7.5	-
$C_{chalcopyrite}$	0.5	-
C_{pyrite}	0.75	-
$\rho_{chalcopyrite}$ (Ohm-m)	0.004	-
ρ_{pyrite} (Ohm-m)	0.3	-
$a_{chalcopyrite}$ (mm)	0.2, 0.5, 0.7, 1, 1.2, 1.5, 2, 3	0.2-0.5, 0.5-1, 1-2, 2-3
a_{pyrite} (mm)	0.2, 0.5, 0.7, 1, 1.2, 1.5, 2, 3	0.2-0.5, 0.5-1, 1-2, 2-3
$\alpha_{chalcopyrite}$ ($\frac{\mathrm{Ohm \cdot m^2}}{\mathrm{sec}^{c_l}}$)	0.85	-
α_{pyrite}	0.5 ($\frac{\mathrm{Ohm \cdot m^2}}{\mathrm{sec}^{c_l}}$)	-

Deposit-scale results

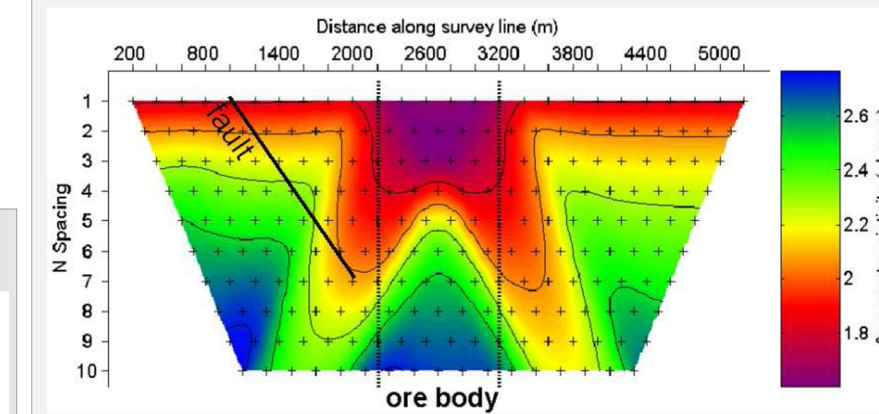

Figure 12: Apparent resistivity pseudosection for 1 Hz data. A pseudosection is created by plotting the computed apparent resistivity as a function of N-spacing and horizontal position. N-spacing refers to the separation of the transmitting dipole and receiving dipole as a multiplier of the dipole spacing. For this 200m dipole-dipole survey configuration an N-spacing of three would indicate the center transmitting dipole is 600 m from the center of the receiving dipole. N-spacing can be difficult to directly correlate with actual depth. A conductivity low blankets the ore body in the center. Influence of the fault is seen in the right side of the psuedosection where the apparent resistivity is higher and creates left to right asymmetry in the response produced by the ore body. This representation of the data is useful in finding the horizontal extent of the ore body, but does not indicate depth to the ore body nor vertical extent. An inversion may be useful to determine these parameters.

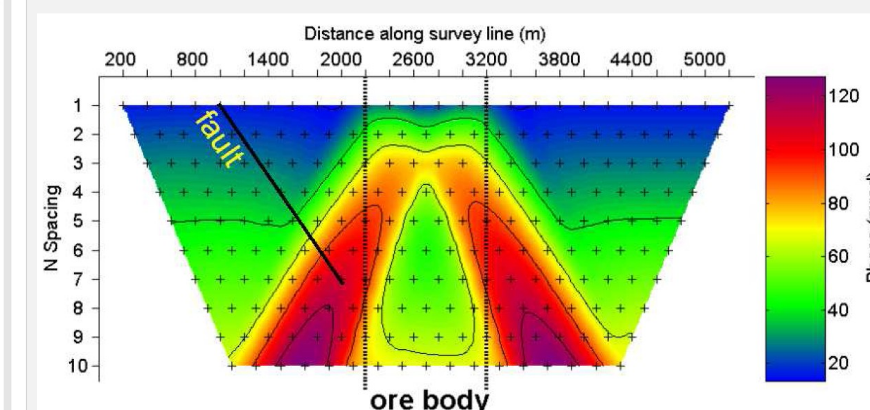

Figure 13: Apparent phase pseudosection for 1 Hz data. Apparent phase is computed from the angle formed between the real and imaginary part of the apparent resistivity. Apparent phase is plotted in the same manner as the apparent resistivity pseudosection. A phase anomaly due to the ore body is symmetric about the center. Phase anomalies can indicate the presence of sulfide mineralization. Influence of the fault is not seen in the phase data as it does not have a strong IP response. Again, this representation of the data is useful in finding the horizontal extent of the ore body, but does not indicate depth to the ore body or vertical extent.

Table 4: Modeling parameters for synthetic data presented in figures 12 and 13.

survey type	2-D 200 m dipole dipole
survey length	5000 m
Tx Rx pairs	351
frequencies	0.125, 0.5, 1, 4, 8, and 16 Hz
conductivity model	complex (kcomp = 1)
Anomalous Body	2000 cells
IBC Body	2000 cells
PC Time	1 hour
PC Type	1.4 GHz Athlon, 1 GB RAM

Summary and future work

Recent developments in IP theory and forward modeling have opened the door to further our understanding the IP effect in both mineral and petroleum exploration leading to better detection and discrimination capabilities. The development of GEMTIP now allows the inclusion of rock-scale parameters such as mineralization and/or fluid content, matrix composition, porosity, anisotropy, and the polarizability of the formations. The capability to model the IP effect on the rock-scale in maturing.

Initial testing shows GEMTIP is able to fit empirical data. As with any new concept, additional comparisons will be necessary to test the robustness of the GEMTIP model. Rock-scale measurements will be conducted in the summer of 2006.

To further understand a porphyry system through electromagnetic forward modeling, a simplified porphyry model was created for use with the IBCEM3DIP code. Using the simple porphyry model and code, optimal survey configuration and ore body detectability can be studied.

Acknowledgments

This work was supported by the National Energy Technology Laboratory of the U.S. Department of Energy under contract DE-FC26-04NT42081 and by the following members of the MDCA project: BHP Billiton World Exploration Inc., Kennecott Exploration Company, Placer Dome, Phelps Dodge Mining Company, and Zonge Engineering and Research Organization Inc. The authors also acknowledge the support of the University of Utah Consortium for Electromagnetic Modeling and Inversion (CEMI), which includes BAE Systems, Baker Atlas Logging Services, BGP China National Petroleum Corporation, BHP Billiton World Exploration Inc., Centre for Integrated Petroleum Research, EMGS, ENI S.p.A., ExxonMobil Upstream Research Company, INCO Exploration, Information Systems Laboratories, MTEM, Newmont Mining Co., Norsk Hydro, OHM, Petrobras, Rio Tinto - Kennecott, Rocksource, Schlumberger, Shell International Exploration and Production Inc., Statoil, Sumitomo Metal Mining Co., and Zonge Engineering and Research Organization. We are thankful to Seong Kon Lee and Takumi Ueda for developing theIBCEM3DIP forward modeling code, to Alex Gribenko for assistance with original GEMTIP modeling, and to Ken Yoshioka for help with visualization codes.

Special thanks to the Society of Economic Geologists for providing funding for this poster presentation.

References

Cole, K. S., and Cole, R. H., 1941, Dispersion and absorption in dielectrics, J. Chem. Phys., 9, 343-351.

Nabighian, M. N., 1988, Electromagnetic Methods in Applied Geophysics, Electromagnetic methods in applied geophysics, 01: Soc. of Expl. Geophys., 528.

Ostrander, A. G., and Zonge, K. L., 1978, Complex Resistivity Measurements of Sulfide-Bearing Synthetic Rocks: 48th Ann. Internat. Mtg., Soc Expl. Geophys., Expanded Abstracts.

Pelton, W. H., Ward, J. G., Hallof, J. G., Sill, W. R., and Nelson, P. H., 1978, Mineral discrimination and removal of inductive coupling with multifrequency IP: Geophysiccs, 43, 588-609.

Pierce, F. W., and Bolm, J. G , eds., 1995, Porphyry Copper Deposits of the American Cordillera: Arizona Geological Society Digest 20.

Sillitoe, R. H., 1973, The tops and bottoms of Porphyry Copper Deposits: Econ. Geol., 68, 799-815.

Titley, S. R., ed., 1982, Advances in Geology of the Porphyry Copper, Southwestern North America, University of Arizona Press, Tucson, AZ

Zhdanov, M. S., 2006, Generalized effective medium theory of the complex resistivity of multi-phase heterogeneous rocks: Proc. Ann. Mtg., Consortium for Electromagnetic Modeling and Inversion. 1-24.

Zhdanov, M. S., and Lee, S. K., 2005, Integral equation method for 3-D modeling of electromagnetic fields in complex structures with inhomogeneous background conductivity: 75th Ann. Internat. Mtg., Soc. Expl. Geophys., Expanded Abstracts. 16